# Voltage stability index-based reactive power compensation scheme ☆

Damian O. Dike [a,*], Satish M. Mahajan [b]

[a] Electrical and Electronic Engineering Department, Federal University of Technology, Owerri, Nigeria
[b] Tennessee Technological University, Cookeville, USA

A B S T R A C T

Reports of various committees set up to review the 2003 North American major power outages pointed out that a major exacerbating factor has been lack of situational awareness by power system operators. To improve reactive power compensation and contribute to the mitigation of power outages associated with the present near-limit operated commercialized grid, a bus voltage stability (BVS) index based reactive power compensation scheme has been developed. BVS index is a hybrid voltage stability computation model involving the two machine modeled L-index and a complex power Π-transmission line structure modeled Ls-index developed by the authors. The current regional wheeling of power across transmission distance far beyond the two machine model has necessitated the development of a novel Ls-index model suitable for long lines. The composite scheme was then incorporated into Newton–Raphson's (N–R) power flow which encompasses multiple shunt devices (multi-shunt). This arrangement provided a knowledge based system for power system monitoring. Results obtained from applying the developed models and schemes in the IEEE 300 bus system with zoning and under varying operating conditions showed the system's capability to provide improved system monitoring and optimal compensation based on availability.

## Introduction

With growing concern for voltage instability and the need to improve power system performance to meet load demand occasioned by deregulation, the industry has focused attention on providing greater reactive support to the distressed grid [1–3]. Consequently, Flexible AC Transmission Systems (FACTS) and distributed energy resources (DERS) in the form of microgrids have also been utilized [4–15]. The basic categories of precipitating events or causes of the August 14th 2003 North American blackout were: (i) "inadequate situational awareness" on the part of FirstEnergy; (ii) FirstEnergy's failure to "manage adequately tree growth in its transmission right-of-way"; and (iii) "failure of the interconnected grid's reliability organizations to provide *effective diagnostic support*" [16]. In view of this report and those of other large scale power system outages [17–22], which started occurring since this period of deregulation and inception of modern reactive compensation schemes there is the utmost need to develop an improved power system status indicator. The status indicators could be in the form of thermal stability or voltage stability. However, since this research is focused primarily on reactive power compensation which is directly related to the power system voltage, this work dwells on the voltage stability based index. Existing voltage stability index models have been presented in [23,24].

Considering the medium and long distance bulk wheeling of power between various independent system operators (ISOs), regional transmitting organizations (RTOs) and over international boundaries, a novel bus VSI (Ls-index) suitable for medium and long transmission line application using the Π-complex transmission line model was developed [25–27]. The results obtained from applying Ls-index had been compared with L-index developed using two-machine transmission line model [24,26]. The results showed the effect of interconnecting transmission line distances on power system stability status [24]. In this paper, a hybrid voltage stability index scheme will be presented after combining the applications of L-index and Ls-index since most power system networks are composed of a mix of short, medium and long transmission lines.

This hybrid scheme will be applied with the Newton Raphson's (N–R) power flow model to determine the weak buses that require compensation. Thereafter, shunt FACTS device will be included in

the N–R power flow model. With this new model, a new load flow result will be obtained and used to compute the hybrid voltage stability index. This will give an independent indication of power system status which can be read to determine the impact of the reactive compensation on the entire network. The compensation device can be set appropriately and if it is not given the desired support, it may be replaced.

The same philosophy may be applied to the transmission line voltage stability index models [26] and used to determine the lines which need compensation, the level of compensation required, and the effects on a selected portion, or the entire interconnected network. Some of the formulations and selection criteria as discussed by the authors earlier [26,27] with IEEE 14 and 30 bus system was modified and incorporated in the IEEE 300 bus system. The algorithm developed here also includes a feature to sub-divide large networks into groups to enhance faster operation and closer monitoring. It is hoped that the outcome of this work will provide efficient tools for the determination of power system status, ensure optimal utilization of the dynamic reactive power compensation devices, and reduce system outages through improved system monitoring.

The paper is arranged in the following manner. Section 'Justification for the use of voltage stability index in facts schemes' presents justifications for the introduction of an independent monitoring index in the power system compensation scheme. In Section 'Modeling of long transmission system bus voltage stability index', modeling of both the bus voltage stability index and the selected transmission line stability indexes are depicted. Section 'Scheme implementation algorithm' contains the development of implementation algorithm. Section 'Results and discussions' exhibits simulated results for the test system and accompanying discussions. Finally, the conclusions are given in Section 'Conclusion'.

## Justification for the use of voltage stability index in facts schemes

To be able to address the two critical issues stated as the major causes of the 2003 blackout – "inadequate situational awareness" and "failure of the interconnected grid's reliability organizations to provide effective diagnostic support" [16], it is important to examine further the operational limitations of reactive power compensation devices as applied to the present power system.

### Cost of FACTS devices

The cost of procurement, installation and maintenance of most of the FACTS devices are exorbitant and therefore, economically non-viable. Though SSSC, UPFC, IPFC and GUPFC have been tested in pilot projects [28,29], cases of practical installation are very insignificant. This has left system operators to continue making use of the simple and relatively cheap compensation devices like the SVC and the STATCOM as well as their offshoots [30–36]. Therefore, there is a need to incorporate status monitoring devices which will also guide in the appropriate utilization of these preferred devices.

### Compensation devices not suitable for faulty operating conditions

Most compensation devices like the TCR, SVC STATCOM, TCSC and SSSC are designed to operate under specified limits. These limits correspond to their normal operating conditions. However, during faulty conditions in the network which are outside the operational limits, these devices give unreliable results. Due to the fast varying load types and near limit operating conditions of current power systems, there is a need to incorporate an additional status monitoring scheme. Doing this will help in the early determination of some of these abnormal situations.

### Effect of reactive power compensation not localized

Generally, the present day power systems are composed of interconnected complex transmission lines, transformers, network compensators and varied types of load and generator buses spanning regional and international barriers. To ensure that the realization of the two basic objectives of power system compensation, namely, increasing the power transfer capability of transmission systems and keeping power flow over designated routes [29], thyristor switches are utilized to control the combined reactive impedance of both the capacitor and reactor banks.

## Modeling of long transmission system bus voltage stability index

In an earlier effort to estimate the voltage stability of a power system, a two machine transmission line structure was used to develop a short line voltage stability indicator (L-index) [23]:

$$L_j = \max_{j \in \alpha_L} \left| 1 - \frac{\sum_{i \in \alpha_G} F_{jk} V_k}{V_j} \right| \tag{1}$$

where $F_{jk} = -[Y] |Y_{jj}|^{-1}$ (2)

The L-index was validated when it was compared with the voltage ratio index to determine the strength of each of the buses in IEEE 14 bus network [24]. However, the authors went further in [26] to develop an algorithm which made it possible to consider the effect on longer transmission line distances in the voltage stability of a given network.

In view of the long distance bulk wheeling of power between different ISOs and RTOs due to seasonal and hourly difference in power generation and peak load demand as well as reduced cost in remote generations, it became necessary to further consider the effect of transmission line distances on the voltage stability index models [25]. Therefore, a complex long transmission line structure as presented in Fig. 1 was used to develop a new Ls-index.

The line parameters are defined hereunder. Modified total line series impedance,

$$Z' = Z_c \sinh \gamma l = Z \frac{\sinh \gamma l}{\gamma l}$$

Modified total line-neutral admittance $\frac{Y'}{2} = yl = \frac{Y}{2} \frac{\tanh(\gamma l/2)}{\gamma l/2}$

The characteristic impedance and propagation constant are:

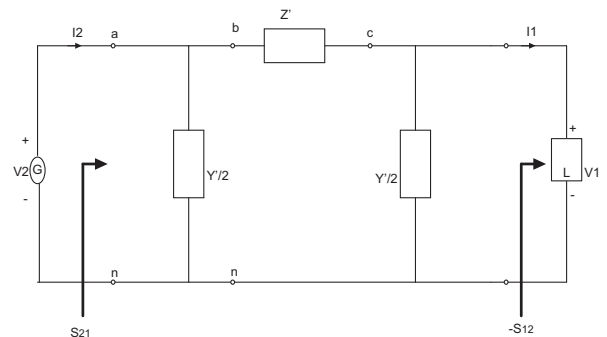$$Z_c = \sqrt{\frac{z}{y}}$$
$$\gamma = \sqrt{yz}$$



**Fig. 1.** Transmission line complex pi-model [25].

For typical power lines,

$$\frac{\sinh \gamma}{\gamma l} \approx 1$$

When detailed line data are not known, the modified total series impedance and line-neutral admittance are taking approximately equal to the total line series line impedance and line-neutral admittance respectively.

*Single-node model*

With the above definitions, the sending end and receiving end complex power are given from [25] as:

$$S_2 = S_{21} = \frac{Y'^*}{2}|V_2|^2 + \frac{|V_2|^2}{Z'^*} - \frac{V_2 V_1}{Z'^*} \tag{3}$$

The receiving end complex power becomes:

$$S_1 = S_{12} = \frac{Y'^*}{2}|V_1|^2 + \frac{|V_1|^2}{Z'^*} - \frac{V_1 V_2}{Z'^*} \tag{4}$$

Eq. (4) represents the complex power at node 1 (load bus) whose voltage is of interest. The basic equations developed in the derivation of medium and long transmission line voltage stability index (Ls-index) using similar approach adopted in [26] are presented hereafter.

$$\frac{S_1}{V_1} = \frac{Y'^*}{2}\frac{|V_1|^2 V_1^*}{V_1 V_1^*} + \frac{|V_1|^2 V_1^*}{Z'^* V_1 V_1^*} - \frac{V_2}{Z'^*} \tag{5}$$

$$\frac{S_1}{V_1} = V_1^*\left(\frac{Y'^*}{2} + \frac{1}{Z'^*}\right) - \frac{V_2}{Z'^*} \tag{6}$$

Letting

$$M_{11} = \frac{Y'^*}{2} + \frac{1}{Z'^*}$$

$$M_{12} = \frac{1}{Z'^*}$$

Then,

$$\frac{S_1}{M_{11}} = V_1^* V_1 - \frac{M_{12}V_2}{M_{11}}V_1 = a_1 + jb_{12} \tag{7}$$

Letting $V_{01} = -\frac{M_{12}}{M_{11}}V_2$, Eq. (7) gives,

$$|V_1|^2 + V_{01}V_1^* = \frac{S_1}{M_{11}} = a_1 + jb_1 \tag{8}$$

Defining $V_{01} = x_0 + jy_0$ and $V_1 = x_1 + jy_1$
Eq. (8) gives:

$$|V_1|^2 - a_1 + x_0 x_1 - y_0 y_1 = j(b_1 - x_0 y_1 - y_0 x_1) \tag{9}$$

$$x_0 x_1 - y_0 y_1 = a_1 - |V_1|^2 \tag{10}$$

$$x_0 y_1 + y_0 x_1 = b_1 \tag{11}$$

$$x_0^2 x_1^2 + y_0^2 y_1^2 - 2x_0 x_1 y_0 y_1 = a_1^2 - 2a_1|V_1|^2 + |V_1|^4 \tag{12}$$

$$x_0^2 y_1^2 + y_0^2 x_1^2 + 2x_0 x_1 y_0 y_1 = b_1^2 \tag{13}$$

Adding Eqs. (12) and (13) gives:

$$x_0^2 x_1^2 + y_0^2 y_1^2 + x_0^2 y_1^2 + y_0^2 x_1^2 = a_1^2 + b_1^2 - 2a_1|V_1|^2 + |V_1|^4 \tag{14}$$

$$(x_1^2 + y_1^2)(x_0^2 + y_0^2) = a_1^2 + b_1^2 - 2a_1|V_1|^2 + |V_1|^4 \tag{15}$$

$$|V_1|^2 |V_{01}|^2 = a_1^2 + b_1^2 - 2a_1|V_1|^2 + |V_1|^4 \tag{16}$$

$$|V_1|^2 = \frac{(2a_1 + |V_{01}|^2) \pm \sqrt{(2a_1 + |V_{01}|^2)^2 - 4(a_1^2 + b_1^2)}}{2} \tag{17}$$

$$|V_1| = \sqrt{\frac{|V_{01}|^2}{2} + a_1^2 \pm \sqrt{\left(\frac{|V_{01}|^4}{4} + a_1|V_{01}|^2 - b_1^2\right)}} \tag{18}$$

From [23], it was deduced that the stability limit of the two-node system, which is of interest, lies at the border line satisfying the discriminator of Eq. (18) given as:

$$\sqrt{\left(\frac{|V_{01}|^4}{4} + a_1|V_{01}|^2 - b_1^2\right)} = 0 \tag{19}$$

With the aid of complex transformation, Eq. (19) gives:

$$\left|1 + \frac{V_{01}}{V_1}\right| = 1 \tag{20}$$

Eq. (19) is used to define an index for computation of closeness of load buses to voltage stability limit given as:

$$L_1 = \left|1 + \frac{V_{01}}{V_1}\right| \tag{21}$$

*Multi-node system voltage stability index*

Since a typical power system involves a large number of load buses, the above two machine model has to be extended to cover such a large system. To achieve this, the hybrid (H) matrix scheme has been severally adopted. H-matrix is represented as [23]:

$$\begin{bmatrix} V^L \\ I^G \end{bmatrix} = \begin{bmatrix} Z^{LL} & F^{LG} \\ K^{GL} & Y^{GG} \end{bmatrix} \begin{bmatrix} I^L \\ V^G \end{bmatrix} \tag{22}$$

where

$$H = \begin{bmatrix} Z^{LL} & F^{LG} \\ K^{GL} & Y^{GG} \end{bmatrix} \tag{23}$$

$H_{11} = \sum_{k \in \alpha_L} Z_{jk}$ represents the aggregate impedance connecting other load buses to load bus of focus. $H_{12} = \sum_{k \in \alpha_G} \frac{Y_{jk}}{Y_{jj}}$ is a dimensionless ratio of the net-admittance to the sum of the admittance linking the generator buses to the load bus of interest. With this hybrid matrix, we get the load bus voltage as:

$$V_j = \sum_{k \in \alpha_L} Z_{jk}I_k + \sum_{k \in \alpha_G} \frac{Y_{jk}}{Y_{jj}}V_k \tag{24}$$

Defining $V_{0j} = -\sum_{k \in \alpha_G} \frac{Y_{jk}}{Y_{jj}}V_k$, the present derivation is given by:

$$V_{0j} = -\sum_{k \in \alpha_G} \frac{M_{jk}}{M_{jj}}V_k \tag{25}$$

$$|V_j|^2 + V_{0j}V_j^* = \frac{S_j^*}{Y_j} \tag{26}$$

Therefore, for a given load bus $j$ in a multi-system, its proximity to collapse could be computed similar to that for two machine model as:

$$L_j = \left|1 + \frac{V_{0j}}{V_j}\right| \tag{27}$$

Hence, a new generalized index for computation of proximity to voltage collapse for load buses in medium and long lines which are the predominant cases in power pooling could be written as:

$$L_{sys} = \sum_{l \in \alpha_L} \max\left|1 - \frac{\sum_{k \in \alpha_G} \frac{M_{lk}}{M_{ll}}V_k}{V_l}\right| \tag{28}$$

*Modification of the original L-index*

To further make the computation of the bus voltage collapse index L-index, consideration of the fact that the net contribution

resistance to the impedance of the medium and long transmission lines to the self-admittance of each bus is negligible when compared with that of the reactance. Therefore, the hybrid term of $F_{ji} = -[Y_{jj}]^{-1}Y_{ji}$ was reduced to $F_{ji}^1 = -[B_{jj}]^{-1}Y_{ji}$. When this was substituted in the formulation for the L-index, we now obtain:

$$L_S = \max_{j\in\alpha_L}\{L_j\} = \max_{j\in\alpha_L}\left|1 - \frac{\sum_{i\in\alpha_G}F_{ji}^1 V_k}{V_l}\right| \quad (29)$$

*Inclusion of shunt facts devices in the Newton–Raphson's load flow model*

*Newton's power flow model*

The basic real and reactive power flow equations for a transmission line between buses 'p' and 'q' as:

$$P_p = \sum_{q=1}^{N}|V_p||V_q|(G_{pq}\cos\theta_{pq} + \mathbf{B}_{pq}\sin\theta_{pq}) \quad (30)$$

$$Q_p = \sum_{q=1}^{N}|V_p||V_q|(G_{pq}\sin\theta_{pq} - \mathbf{B}_{pq}\cos_{pq}) \quad (31)$$

For $p = 1, 2, 3 \ldots N$.

The Newton power flow equation in polar coordinate is written as:

$$\begin{bmatrix} \frac{\partial P_p}{\partial\theta_p} & \frac{\partial P_p}{\partial V_p} \\ \frac{\partial Q_p}{\partial\theta_p} & \frac{\partial Q_p}{\partial V_p} \end{bmatrix}\begin{bmatrix} \Delta\theta_p \\ \Delta V_p \end{bmatrix} = -\begin{bmatrix} \Delta P_p \\ \Delta Q_p \end{bmatrix} \quad (32)$$

*Multi-STATCOM structure in Newton power flow*

Fig. 2 represents a simplified power system having multiple STATCOM devices (herein referred to as Multi-STATCOM). Equations representing real and reactive the power exchange between the bus and STATCOM are given by:

$$P_{sh} = V_p^2 G_{sh} - V_p V_{sh}(G_{sh}\cos(\theta_p - \theta_{sh}) - B_{sh}\sin(\theta_p - \theta_{sh})) \quad (33)$$

$$Q_{sh} = -V_p^2 G_{sh} - V_p V_{sh}(G_{sh}\sin(\theta_p - \theta_{sh}) - B_{sh}\cos(\theta_p - \theta_{sh})) \quad (34)$$

Because STATCOM is primarily utilized for reactive power compensation or bus voltage enhancement, a major consideration is to ensure that the net active power exchange is made close to zeros as much as possible to ensure maximum reactive power flow. Hence, active power exchange (PE) becomes a control given as:
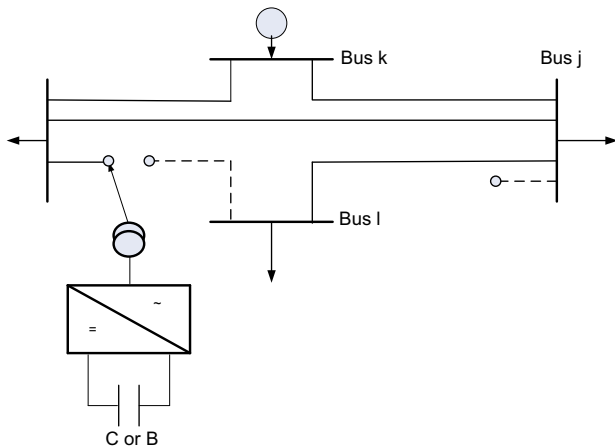


**Fig. 2.** Multi-STATCOM in power system network.

$$PE = P_{sh}$$
$$= V_p^2 G_{sh} - V_p V_{sh}(G_{sh}\cos(\theta_p - \theta_{sh}) - B_{sh}\sin(\theta_p - \theta_{sh})) = 0 \quad (35)$$

Eq. (34) is one of the two equations required for the inclusion of STATCOM in the power flow model of Newton's equation.

*Utilizing STATCOM power system control functions*

The second important equation is selected from one of the STATCOM control functions $F(x)$ given in Eqs. (36)–(42).

(a) Control of reactive power injection to connected bus given by:
$$Q_{sh} - Q_{sh}^{spec} = 0 \quad (36)$$
where $Q_{sh}$ is as stated in Eq. (34).

(b) Control of load bus voltage magnitude:
$$V_p - V_p^{spec} = 0 \quad (37)$$

(c) Control of equivalent STATCOM injected voltage magnitude
$$V_{sh} - V_{sh}^{spec} = 0 \quad (38)$$

(d) Control of STATCOM reactive impedance
$$X_{pq} - X_{pq}^{spec} = 0 \quad (39)$$

(e) Control of leading or lagging current magnitude
The capacitive (leading current) control mode is given by:
$$Re(I_{sh}^{spec}\angle(\theta_{sh} + 90°)) = Re((V_p - V_{sh})/Z_{sh})$$
$$\Rightarrow Im(I_{sh}^{spec}\angle(\theta_{sh}^{spec} + 90°))$$
$$= Im((V_p - V_{sh})/Z_{sh}) \quad (40)$$

Inductive (lagging current) control mode is represented as:
$$Re(I_{sh}^{spec}\angle(\theta_{sh} - 90°)) = Re((V_p - V_{sh})/Z_{sh})$$
$$\Rightarrow Im(I_{sh}^{spec}\angle(\theta_{sh}^{spec} - 90°))$$
$$= Im((V_p - V_{sh})/Z_{sh}) \quad (41)$$

(f) Control of local load bus apparent power:
$$S_{pq} - S_{pq}^{spec} = 0 \quad (42)$$

The control functions of the STATCOM of Eqs. (36)–(42) are combined to get the generalized control function denoted as:

$$\Delta E(x) = E(x) - E(x)^{spec} \quad (43)$$

where $x = [\theta_p, V_p, \theta_{sh}, V_{sh}]$.

*Derivation of the STATCOM Jacobian matrix*

In the formulation of the Jacobian matrix of the STATCOM, the equations used are the active power net-zeros exchange of Eq. (35) and the STATCOM reactive power given in Eq. (36). Adding the partial derivatives of these two equations into the Newton's Jacobian matrix of Eq. (32), we obtained the generalized multi-STATCOM Jacobian as indicated in Eq. (44).

$$[J] = \begin{bmatrix} \frac{\partial P_p}{\partial\theta_p} & \frac{\partial P_p}{\partial V_p} & \frac{\partial P_p}{\partial\theta_{sh}} & \frac{\partial P_p}{\partial V_{sh}} \\ \frac{\partial Q_p}{\partial\theta_p} & \frac{\partial Q_p}{\partial V_p} & \frac{\partial Q_p}{\partial\theta_{sh}} & \frac{\partial Q_p}{\partial V_{sh}} \\ \frac{\partial PE}{\partial\theta_p} & \frac{\partial PE}{\partial V_p} & \frac{\partial PE}{\partial\theta_{sh}} & \frac{\partial PE}{\partial V_{sh}} \\ \frac{\partial E}{\partial\theta_p} & \frac{\partial E}{\partial V_p} & \frac{\partial E}{\partial\theta_{shq}} & \frac{\partial E}{\partial V_{sh}} \end{bmatrix} \quad (44)$$
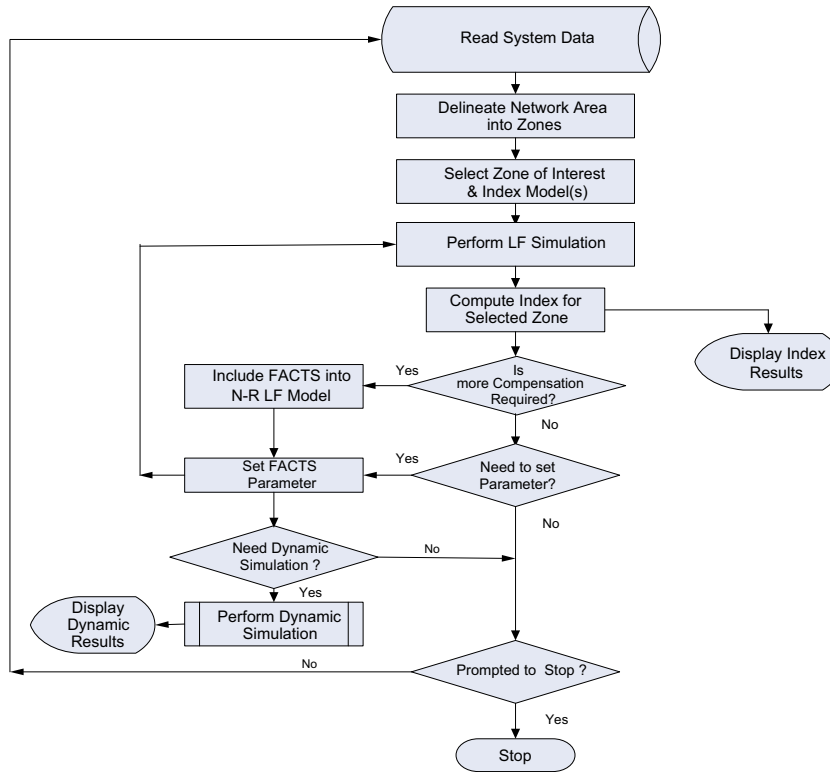
**Fig. 3.** Voltage stability index FACTS scheme implementation algorithm.

where $[J] = \begin{bmatrix} J1 & J2 & J3 & J4 \\ J5 & J6 & J7 & J8 \\ J9 & J10 & J11 & J12 \\ J13 & J14 & J15 & J16 \end{bmatrix}$.

The unique arrangement of the multi-STATCOM Jacobian matrix above to ensure a complete load flow program for implementation of a power system network having more than one STATCOM interconnected is illustrated by the expansion of the Jacobian of (44) into (45).

However, to consider situations where more than one STATCOM are installed in networks, each of the $J$ terms in Eq. (45) should be made to vary according to the number of buses in the network. To speed up computation and save storage space, the program was developed to avoid computations involving zeros and the each result stored in sparse form.

$$[J_{\exp}] = \begin{bmatrix} \frac{\partial P_1}{\partial \theta_1} & \cdot & \cdot & \frac{\partial P_1}{\partial \theta_{N-1}} & \frac{\partial P_1}{\partial V_1} & \cdot & \frac{\partial P_1}{\partial V_{N-1}} & \frac{\partial P_1}{\partial \theta_{sh}} & \frac{\partial P_1}{\partial V_{sh}} \\ \cdot & \cdot & \cdot & \cdot & \cdot & \cdot & \cdot & \cdot & \cdot \\ \cdot & \cdot & \cdot & \cdot & \cdot & \cdot & \cdot & \cdot & \cdot \\ \frac{\partial P_{N-1}}{\partial \theta_1} & \cdot & \cdot & \frac{\partial P_{N-1}}{\partial \theta_{N-1}} & \frac{\partial P_{N-1}}{\partial V_1} & \cdot & \frac{\partial P_{N-1}}{\partial V_{N-1}} & \frac{\partial P_{N-1}}{\partial \theta_{sh}} & \frac{\partial P_{N-1}}{\partial V_{sh}} \\ \frac{\partial Q_1}{\partial \theta_1} & \cdot & \cdot & \frac{\partial Q_{N-1}}{\partial \theta_{N-1}} & \frac{\partial Q_1}{\partial V_1} & \cdot & \frac{\partial Q_1}{\partial V_{N-1}} & \frac{\partial Q_1}{\partial \theta_{sh}} & \frac{\partial Q_1}{\partial \theta_{sh}} \\ \cdot & \cdot & \cdot & \cdot & \cdot & \cdot & \cdot & \cdot & \cdot \\ \cdot & \cdot & \cdot & \cdot & \cdot & \cdot & \cdot & \cdot & \cdot \\ \frac{\partial Q_{N-1}}{\partial \theta_1} & \cdot & \cdot & \frac{\partial Q_{N-1}}{\partial \theta_{N-1}} & \frac{\partial Q_{N-1}}{\partial V_1} & \cdot & \frac{\partial P_{N-1}}{\partial V_{N-1}} & \frac{\partial Q_{N-1}}{\partial \theta_{sh}} & \frac{\partial Q_{N-1}}{\partial V_{sh}} \\ \frac{\partial PE}{\partial \theta_1} & \cdot & \cdot & \frac{\partial PE}{\partial \theta_{N-1}} & \frac{\partial PE}{\partial V_1} & \cdot & \frac{\partial PE}{\partial V_{N-1}} & \frac{\partial PE}{\partial \theta_{sh}} & \frac{\partial PE}{\partial V_{sh}} \\ \frac{\partial E}{\partial \theta_1} & \cdot & \cdot & \frac{\partial E}{\partial \theta_{N-1}} & \frac{\partial E}{\partial V_1} & \cdot & \frac{\partial E}{\partial V_{N-1}} & \frac{\partial E}{\partial \theta_{sh}} & \frac{\partial E}{\partial V_{sh}} \end{bmatrix}$$

(45)
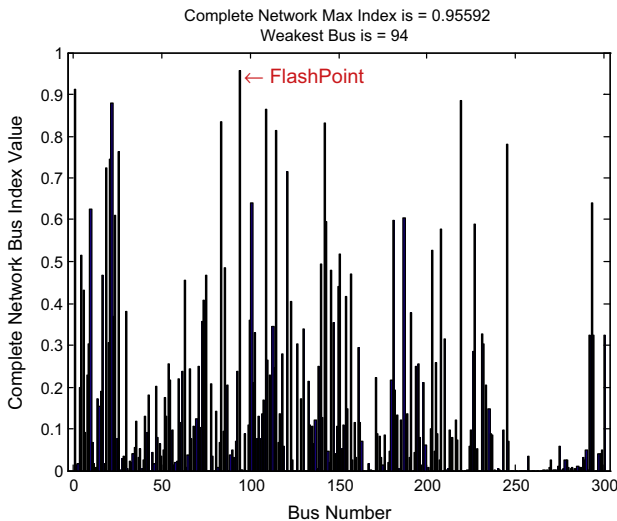


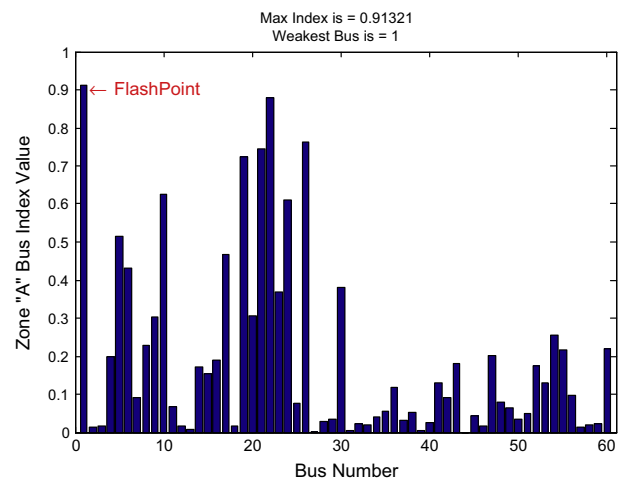**Fig. 4.** Bus voltage stability index for IEEE 300 bus.



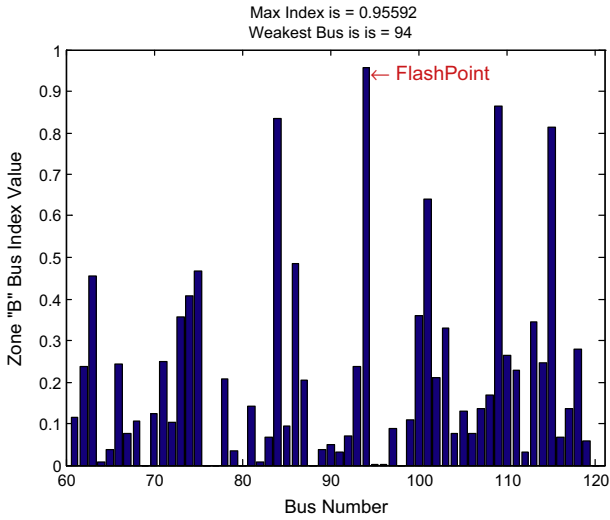**Fig. 5.** Bus voltage stability index for IEEE 300 bus (Zone A).

**Fig. 6.** Bus voltage stability index for IEEE 300 bus (Zone B).

With this arrangement of the Jacobian, the Newton power flow equation in polar coordinate now becomes:

$$[J]\begin{bmatrix} \Delta\theta_1 \\ . \\ . \\ \Delta\theta_{N-1} \\ \Delta V_1 \\ . \\ . \\ \Delta V_{N-1} \\ \Delta\theta_{sh} \\ \Delta V_{sh} \end{bmatrix} = -\begin{bmatrix} \Delta P_1 \\ . \\ . \\ \Delta P_{N-1} \\ \Delta Q_1 \\ . \\ . \\ \Delta Q_{N-1} \\ \Delta PE \\ \Delta E \end{bmatrix} \quad (46)$$

$$\begin{bmatrix} \Delta\theta_1 \\ . \\ . \\ \Delta\theta_2 \\ \Delta V_1. \\ . \\ \Delta V_{N-1} \\ \Delta\theta_{sh} \\ \Delta V_{sh} \end{bmatrix} = -([J])^{-1}\begin{bmatrix} \Delta P_1 \\ . \\ . \\ \Delta P_{N-1} \\ \Delta Q_1 \\ . \\ . \\ \Delta Q_N \\ \Delta PE \\ \Delta E \end{bmatrix} \quad (47)$$

In the above derivation, the known quantities are:

$$P_p = P_p^{gen} - P_p^{load} \quad (48)$$

$$Q_p = Q_p^{gen} - Q_p^{load} \quad (49)$$

$$P_p^{cal}(x) = \sum_q^N V_p V_q (G_{pq}\cos(\theta_p - \theta_q) + B_{pq}\sin(\theta_p - \theta_q)) \quad (50)$$

$$Q_p^{cal}(x) = \sum_q^N V_p V_q (G_{pq}\sin(\theta_p - \theta_q) - B_{pq}\cos(\theta_p - \theta_q)) \quad (51)$$

$$\Delta P_p = P_p - P_p^{cal}(x) \quad (52)$$

$$\Delta Q_p = Q_p - Q_p^{cal}(x) \quad (53)$$

$$\Delta E = E(x) - E(x)^{spec} \quad (54)$$

$$\Delta PE = PE(x) - PE^{spec} \quad (55)$$

In the matrix form, this can be written as:

$$\begin{bmatrix} \theta_1^{t+1} \\ . \\ . \\ \theta_{N-1}^{t+1} V_1^{t+1} \\ . \\ . \\ V_{N-1}^{t+1} \\ \theta_{sh}^{t+1} \\ V_{sh}^{t+1} \end{bmatrix} = \begin{bmatrix} \theta_1^t \\ . \\ . \\ \theta_N^t \\ V_{N-1}^t \\ . \\ . \\ V_{N-1}^t \\ \theta_{sh}^t \\ V_{sh}^t \end{bmatrix} + \begin{bmatrix} \Delta\theta_1^t \\ . \\ . \\ \Delta\theta_{N-1}^t \\ V_1^t \\ . \\ . \\ V_{N-1}^t \\ \Delta\theta_{sh}^t \\ \Delta V_{sh}^t \end{bmatrix} \quad (56)$$

This was then checked for limits. If violated then reset the limits and the load flow run till convergence was achieved. In running the program, the row and column entries relating to the slack bus were deleted since its voltage was already known.

### Scheme implementation algorithm

The implementation process involved development of the power system Newton–Raphson's load flow model equations with both the load bus voltage stability indexes. Then an associated MATLAB based program was developed and simulated to determine the stability status of the required load bus or the transmission line. A summarized operational algorithm is shown in Fig. 3.
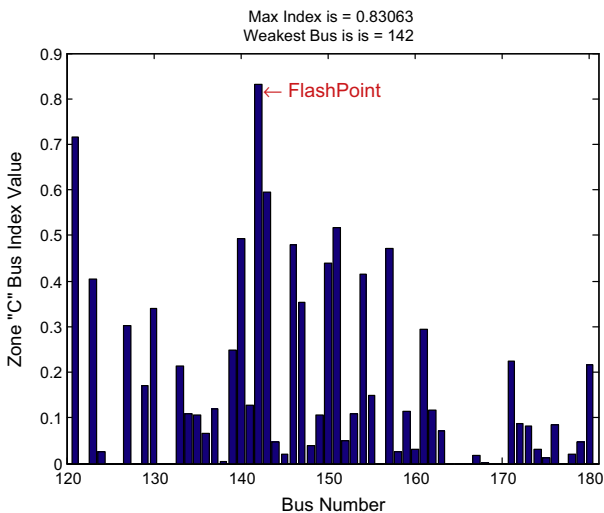


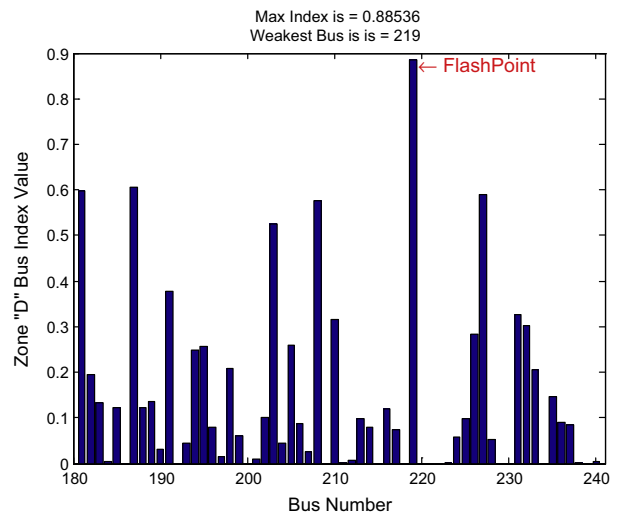**Fig. 7.** Bus voltage stability index for IEEE 300 bus (Zone C).



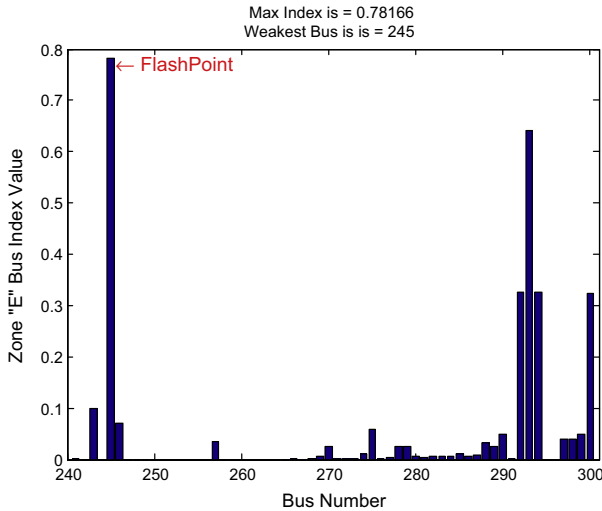**Fig. 8.** Bus voltage stability index for IEEE 300 bus (Zone D).

**Fig. 9.** Bus voltage stability index for IEEE 300 bus (Zone E).

A decision was made based on the computed status from index value whether there is any bus or line within the zone of interest that requires compensation. If there is, then appropriate shunt device was incorporated into the N–R load flow model. The next step involved checking for the settings of the FACTS devices. At this point the system asks if the operator requires dynamic simulation or a re-run of the load flow steady state simulation. The FACTS values continue thereby ensuring that the power system runs in optimal conditions. The simulation stops when prompted.

## Results and discussions

The bus voltage stability status obtained from the steady state MATLAB power flow program using Newton Raphson's approach for the entire IEEE 300 bus system is depicted in Fig. 4.

An index of '1' indicates that the bus is definitely unstable while a value of '0' indicates extreme stability. The weakest bus is denoted as "Flashpoint", and it is prone to initiate system outage. The corresponding bus number and its operating status are indicated at the top of the plot.

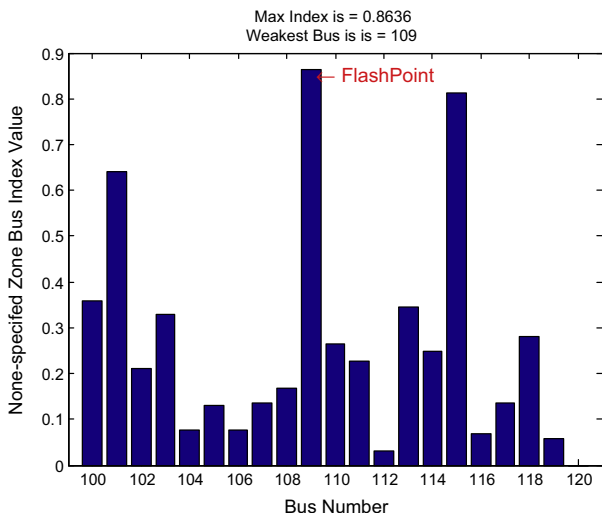To increase the efficiency of the computation scheme and show the dynamism of the developed model to adequately provide wide area monitoring of any network size, the entire network was grouped into five zones. Each of the zones had a span comprising 60 buses and the zones were arranged sequentially from 'A' through 'E'. The results obtained are classified under normal system, 10% overloaded with base STATCOM setting and overloaded with increased STATCOM magnitude.

### Normal system loading

The results obtained for the five zones under base loading are depicted in Figs. 5–9. Provision was also made to accommodate further zonings or special interest re-arrangement of the network. This feature is ably captured in the result displayed in Fig. 10 where only part of zone "B" ranging from bus 100 to bus 120 is shown.

As in the result for the entire network, the developed scheme also shows the weakest load bus, its index values and gives a "FlashPoint" for each zone or off-zone selected. The scheme has the capability of ensuring that the compensation is directed at the actual weakest bus in case the operator was not able to give the correct value. It picks up the weakest bus for the entire network.

The data acquisition component of the program has subroutines that automatically change the status of a bus from generator bus to load bus and vice versa depending on the net loading value and takes care of the double lines in the network. The buses with zero index values are either generator buses or close to the generators. As expected, the load buses close to the generator buses gave very stable values.

The buses with zero indexes are those whose net generations are greater than their current load demand, while those close to zero are very stable. Based on the preliminary results displayed under the current loading arrangement, the buses that required immediate compensation and their zones are displayed in Table 1.

Based on Table 1 and the work done by the authors in [26,27,37], only buses 1 and 94 may be compensated as their indexes are pretty close to the stability margin which each controlling authority may set according to the level of system security desired.

### STATCOM with 10% increased loading

With a STATCOM placed in buses 1 and 94 respectively, and 10% increased system loading, a new set of voltage stability indexes were computed for the entire system as presented in Fig. 11.

The summary of the status of all the zones with the 10% increased loading and installation of STATCOM in buses 1 and 94 are as indicated in Table 2. The indexes of buses 1 and 94 dropped to very stable values, while bus 174 became the new weakest bus for the entire system.

So the effect of placing STATCOM at buses 1 and 94 and increased loading were felt by the entire system. Other zonal stability values presented subsequently further confirmed these findings.



**Fig. 10.** Bus voltage stability index for IEEE 300 bus (off Zone part of B).

**Table 1**
Instability of IEEE 300 bus system by zone.

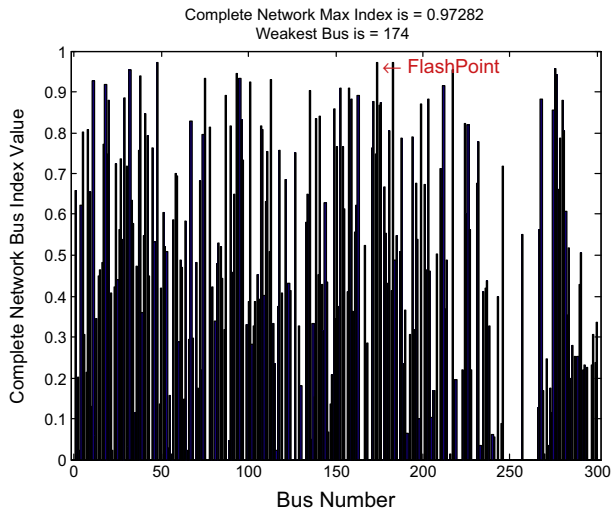| Focus area | Bus no. | Max index | Bus range |
|---|---|---|---|
| Entire N/W | 94 | 0.955920 | 1–300 |
| Zone A | 1 | 0.910210 | 1–60 |
| Zone B | 94 | 0.955920 | 61–120 |
| Zone C | 142 | 0.830630 | 121–180 |
| Zone D | 219 | 0.885360 | 181–240 |
| Zone E | 241 | 0.781660 | 241–300 |
| Off-Zone "B" | 109 | 0.863600 | 100–120 |

**Fig. 11.** Bus voltage stability index for IEEE 300 bus with STATCOM and 10% increased loading.
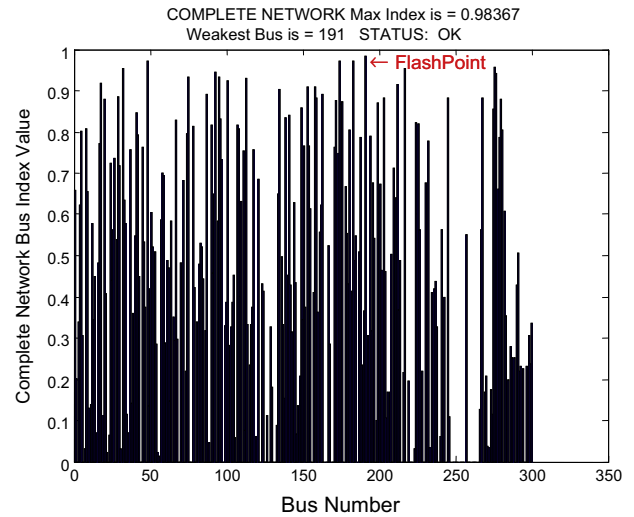


**Fig. 13.** Bus voltage stability index for IEEE 300 bus with 20% increased loading and STATCOM on bus 191.

**Table 2**
Instability of IEEE 300 bus system by zone with STATCOM and 10% increased loading.

| Focus area | Bus no. | Max. index | Bus range |
|---|---|---|---|
| Entire N/W | 174 | 0.972820 | 1–300 |
| Zone A | 48 | 0.971351 | 1–60 |
| Zone B | 93 | 0.945930 | 61–120 |
| Zone C | 174 | 0.972820 | 121–180 |
| Zone D | 183 | 0.971110 | 181–240 |
| Zone E | 276 | 0.957030 | 241–300 |
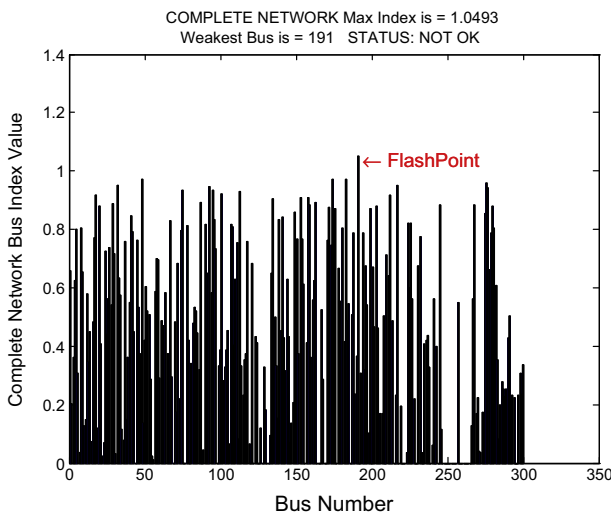


**Fig. 12.** Bus voltage stability index for IEEE 300 bus with 20% increased loading.

Fig. 12 shows results obtained when the loading was increased to 20% with the other operating conditions unchanged as compared to those in Fig. 11. Such a loading produced a voltage collapse situation on bus 191 with an index value of 1.05. The situation was remedied in the simulation for Fig. 13 when STATCOM was on added bus 191.

An optimal voltage stability limit of 0.97 was chosen based on previous results obtained in related works [23,24] and which were corroborated by authors in the earlier work [26,27,30]. Zones 'B' and 'E' had maximum index of 0.94593 and 0.95703 respectively.

The status indicator continues to flash that these two zones do not need any further compensation. Further simulation performed with STATCOM installed on buses 48, 174 and 183 of zones 'A', 'C' and 'D' respectively indicated a fairly improved stability levels of not just the load buses were installed but had much more effect on the adjoining buses and on the entire network.

## Conclusion

A voltage stability-index based shunt compensation scheme and its accompanying algorithm have been developed and applied to rank the load buses of the IEEE 300 bus system according to their vulnerability to outages. It was observed that by splitting the entire network into five zones the simulation speed increased thereby indicating the practical applicability of the developed scheme. Results obtained agreed with similar work done previously.

The results presented in this work demonstrate the best locations and ratings for the FACTS devices. The proposed scheme may reduce problems faced by network operators in regulating future interconnection of FACTS devices and monitoring the performances of their power grid. Apart from system monitoring, it will also enhance proper system planning and control. The scheme can easily be adapted to dynamic operation and also indicate the effect of applied compensation in all parts of the network.

Further research work will be required to implement this scheme in a parallel computer simulation system where each program segment will be performed by different processors with a master controller co-coordinating the overall decision making process of the VSC. The simulation should also be performed under diverse power system operating conditions to reaffirm its robustness.

## References

[1] Kundur P, Paserba J, Ajjarapu V, Anderson G, Bose A, Canizares C, et al. Definition and classification of power system stability. IEEE Trans Power Syst 2004;19:1387–401.

[2] Kundur P. Power system stability and control. New York: McGraw-Hill; 1994.

[3] Philipson L, Willis HL. Understanding electric utilities and de-regulation. NY: Marcel Dekker Inc.; 1998.

[4] Zhang XP, Rehtanz C, Pal B. In: Flexible AC transmission systems: modeling and control. Berlin Heidelberg Germany: Springer-Verlag; 2006. p. 2–3.

[5] Panda S, Patel RN. Improving power system transient stability with an off-centre location of shunt FACTS devices. J Electr Eng 2006;57(6):365–8.

[6] Shimazaki Y. Model analysis of microgrid cogeneration system zero emission industrial park. In: UPE7 – the 7th international conference on urban planning and environment, Bangkok, Thailand; 2007.

[7] Panagis N, Kiprakis AE, Robin WA, Harrison GP. Centralized and distributed voltage control: impact on distributed generation penetration. IEEE Trans Power Syst 2007;22(1).

[8] Silva JA, Funmilayo HB, Butler-Purry KL. Impact of distributed generation on the IEEE 34 node radial test feeder with overcurrent protection. In: Proc of the 2007 39th North American power symposium. Las Cruces, New Mexico: New Mexico State University; 2007. p. 49.

[9] Cipcigan LM, Taylor PC, Trichakis P. The impact of small scale wind generation on low voltage distribution systems voltage. In: International conf on clean electrical power, Italy; 2007. p. 9.

[10] Feero DE, Dawson DC, Stevens J. Protection Issues of the Microgrid Concept, CERTS. Transmission Reliability Program, Office of Power Technologies, U.S. DOE; 2002. p. 4–9.

[11] Firestone R, Marnay C. Energy Manager Design for Microgrids. Consultant Report by CERTS for the California Energy Commission; 2005. p. 1.

[12] Pecas Lopes JA, Moreira CL, Resende FO. Microgrids black start and islanded operation. In: 15th PSCC, Liege, session 27, paper 4; 2005. p. 2.

[13] Billy C, Heydt G, Langness P, Laughter A, Mann B, Rice M, et al. Sustainable electric power options with attention to native American communities. In: Proc of the 39th North American power symposium. New Mexico State University; 2007. p. 177.

[14] Moreira CL, Pecas Lopes JA. Microgrids dynamic security assessment. In: International conference on clean electrical power, Capri, Italy, May 21st–23rd; 2006. p. 26.

[15] Pecas Lopes JA, Moreira CL, Madureira AG. Defining control strategies for microgrids islanded operation. IEEE Trans Power Syst 2006;21(2):916–24.

[16] United States–Canada power system outage task force, Interim report: causes of the August 14th blackout in the United States and Canada (interim report); November 2003.

[17] U.S.–Canada task force on 14 August 2003 blackout [2003]. The August 14 blackout compared with previous major North America outages. Final report on the August 14th 2003 blackouts in the United States and Canada. p. 103–6.

[18] Storms knock out power to over 600,000 customers in U.S. Northeastern Coast. U.S. DOE Energy Assurance Daily, Wednesday; July 19, 2006.

[19] Biggest blackout in U.S. history. CBS News 1-3; August 15, 2003.

[20] Amin M. Powering the 21st century, we can – and must – modernize the grid. IEEE-U.S.A. Today's Engineer. <http://www.todaysengineer.org/2006/Apr/backscatter.asp>.

[21] Siegel R. Massive power outages cripples Los Angeles. NPR; October 14, 2006.

[22] Amin M. North America's electricity infrastructure: Are we ready for more storms? In: IEEE security & privacy. IEEE Computer Society; 2003. p. 19–25.

[23] Kessel P, Glavitsch H. Estimating the voltage stability of a power system. IEEE Trans Power Deliv 1986;1(3) [PWRD-1].

[24] Reis C, Maciel Barbosa FP. A comparison of voltage stability indices. In: IEEE Melecon, Benalmadena, Spain; 2006.

[25] Bergen AR, Vittal V. In: Power system analysis. Upper Saddle River, New Jersey 07458: Prentice-Hall Inc.; 2000. p. 101, 112.

[26] Dike DO, Mahajan SM, Radman G. Development of versatile voltage stability index algorithm. In: IEEE EPC 2007, Montreal QC, Canada; 2007.

[27] Dike DO, Mahajan SM. L-index based microgrid interconnected power system. In: Proc of IEEE PES general meeting, Pittsburg, PA; July 20–24, 2008.

[28] Zhang DX, Pal B, Rehtanz C. Flexible AC Transmission Systems: Modeling and Control. Berlin Heidelberg, Germany: Springer-Verlag; 2006.

[29] Song YH, Johns AT. Flexible AC Transmission Systems (FACTS). London, United Kingdom: The IEE; 1999.

[30] D-VAR solutions – dynamic VAR support for a more reliable grid. American Superconductor, Inc.; 2007.

[31] Panda S. Improving power system transient stability with an off-centre location of shunt FACTS devices. J Electr Eng 2006;57(6):365–8.

[32] Hochgraf C, Lasseter RH. STATCOM controls for operation with unbalanced voltages. IEEE Trans Ind Appl 1998;13(2).

[33] Nguyen PT, Saha TK. Dynamic voltage restorer against balanced and unbalanced voltage sags: modeling and simulation. In: IEEE PES meeting proc, vol. 1; 6–10 June, 2004. p. 639–44.

[34] Wolf G. Utilities apply new technologies to solve age-old transmission grid problems. T & D World; 2007.

[35] Dynamic reactive power compensation. American Superconductor D-VAR Data Sheet; 2008.

[36] Dynamic voltage restorer. ABB automation power electronic systems; January 2001.

[37] Dike DO, Mahajan SM. L-index modulated voltage source converter. Int J Emerg Electr Power Syst 2008;9(5).